International Core Journal of Engineering Volume 12 Issue 3, 2026
ISSN: 2414-1895 DOI: 10.6919/ICJE.202603_12(3).0046

Study on Fracture Initiation Mechanism of Plane Perforation

Yongjun Fang, Pengfei Zhao

School of Mechanical Engineering, Xi'an Shiyou University, Xi'an 710065, China

Abstract

Aiming at the engineering problems of high fracture pressure, great difficulty in fracturing reconstruction, poor fracture propagation effect of conventional perforation technology and high risk of casing damage in deep shale oil reservoirs, this paper systematically studies the hydraulic fracture initiation mechanism under spiral perforation, fixed-plane perforation and plane perforation technologies by combining theoretical analysis, numerical simulation and physical simulation. Based on linear elastic fracture mechanics, a mechanical model for composite fracture initiation at perforation tips was established. The finite element method was used to analyze the influence laws of key parameters such as perforation phase angle and hole density on fracture initiation pressure, propagation morphology and casing damage. The reliability of numerical simulation results was verified by true triaxial physical model experiments, and finally the optimal process parameter scheme for plane perforation was formed. The research results show that the plane perforation technology is significantly superior to spiral perforation and fixed-plane perforation in reducing formation fracture pressure and improving fracture propagation effect; considering the fracturing effect and casing safety factor comprehensively, the optimal process parameters of plane perforation are 16 holes per meter of hole density and 30° of phase angle. Under these parameters, the formation initiation pressure is as low as 61.2 MPa, the maximum fracture width reaches 5.27 mm, and the casing Mises stress is only 551 MPa, which meets the wellbore integrity requirements. The research results can provide theoretical support and on-site guidance for the optimal design of perforation and fracturing in deep shale oil reservoirs.

Keywords

Plane Perforation; Hydraulic Fracture Initiation; Perforation Parameter Optimization; Casing Damage; Numerical Simulation.

1. Introduction

With the continuous development of oil and gas exploration and development to deep layers, deep shale oil reservoirs show typical characteristics of low porosity and low permeability, high in-situ stress and high fracture pressure. Conventional fracturing reconstruction is faced with technical bottlenecks such as great difficulty in fracture initiation, limited fracture extension and significant near-wellbore effect. As a key link connecting the wellbore and the reservoir, the perforation technology type and parameter design directly determine the initiation morphology, propagation law and final fracturing reconstruction effect of hydraulic fractures, and also have an important impact on the integrity and long-term safety of the casing during fracturing.

At present, scholars at home and abroad have carried out a lot of research on the fracturing influence laws of different perforation technologies. In terms of spiral perforation, Yu Qiangang et al.[1]clarified the fracture initiation and propagation laws of spiral perforation through laboratory experiments and numerical simulation, and revealed the fracturing adaptability of spiral perforation under different reservoir conditions; Wang Xiaohua et al.[2]established a 3D fully coupled numerical model of spiral

ISSN: 2414-1895 DOI: 10.6919/ICJE.202603_12(3).0046

perforation fracturing, and analyzed the mutual interference behavior of competitive propagation of multi-hole fractures. In the field of fixed-plane perforation, Zhao Zhenfeng et al.[3]clarified the influence mechanism of fixed-plane perforation phase angle on the initial fracture morphology of hydraulic fracturing through large-scale true triaxial physical model tests; Wang Suling et al.[4]compared the differences in the influence of fixed-plane perforation and spiral perforation on the casing pressure-bearing capacity. For the plane perforation technology, Weng Dingwei et al.[5]confirmed through large-scale physical simulation experiments that plane perforation can effectively reduce the fracture pressure of horizontal wells and improve the perfection degree of hydraulic fractures; Jiang Shu et al.[6]found that plane perforation can make the fractures of the same cluster of perforations converge into a plane, reduce the near-wellbore tortuosity and promote the balanced extension of multi-cluster fractures.

Existing studies mostly focus on the parameter influence analysis of a single perforation technology, and there is still a lack of systematic comparative research on the three technologies of spiral perforation, fixed-plane perforation and plane perforation, especially the multi-objective optimal design of plane perforation parameters for deep shale oil reservoirs, which is difficult to take into account the dual requirements of fracturing reconstruction effect and wellbore integrity. Based on this, taking the deep shale oil reservoir of Shengli Oilfield as the research object, this paper establishes a hydraulic fracture initiation mechanical model at perforation tips, systematically analyzes the influence laws of different phase angles and hole densities on fracture initiation and propagation and casing damage under the three perforation technologies, verifies the numerical simulation results through true triaxial physical model experiments, and finally forms the optimal plane perforation process scheme, providing technical support for the efficient fracturing reconstruction of deep shale oil reservoirs.

2. Hydraulic Fracture Initiation Mechanical Model and Numerical Simulation Method

Establishment of Numerical Model and Parameter Setting

Taking the 5000 m deep shale oil reservoir of Shengli Oilfield as the research object, a 3D fully coupled finite element model of formation-cement sheath-casing with the size of 1000 m×2000 m×100 m was established, with the mesh division of 40×80×20, as shown in Fig. 1. The tied contact was adopted between the formation, cement sheath and casing in the model, and the displacement constraint was applied to the outer boundary of the formation, and the three-dimensional initial in-situ stress was applied at the same time to simulate the real stress environment of the deep reservoir.

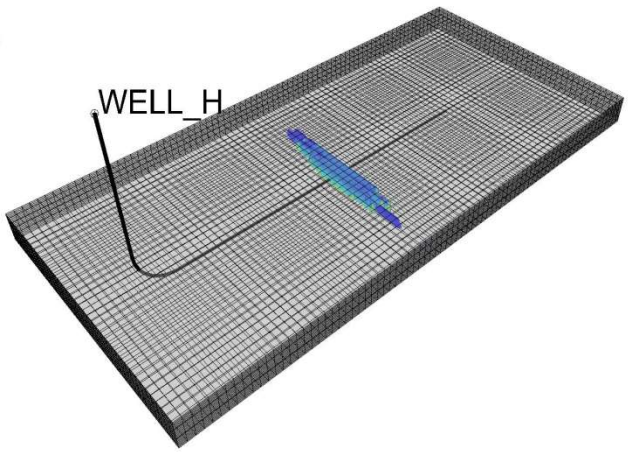

Fig. 1 3D formation model

ISSN: 2414-1895 DOI: 10.6919/ICJE.202603_12(3).0046

The core mechanical parameters of the model are shown in Table 1. The casing is of P110 grade, with an outer diameter of 139.7 mm, a wall thickness of 9.17 mm and a yield strength of 758 MPa; the reservoir rock has an elastic modulus of 30 GPa, a Poisson's ratio of 0.25, a tensile strength of 2.8 MPa, a maximum horizontal principal stress of 110 MPa, a minimum horizontal principal stress of 95 MPa and a vertical stress of 130 MPa, which are consistent with the in-situ stress characteristics of deep shale oil reservoirs.

Table 1. Main parameters of numerical simulation for perforation channel fracturing

Parameter category	Parameter name	Value
Formation rock	Elastic modulus (GPa)	30
	Poisson's ratio	0.25
	Tensile strength (MPa)	2.8
	Maximum horizontal principal stress (MPa)	110
	Minimum horizontal principal stress (MPa)	95
	Vertical stress (MPa)	130
	Pore pressure (MPa)	60
Casing	Outer diameter (mm)	139.7
	Wall thickness (mm)	9.17
	Steel grade	P110
	Elastic modulus (GPa)	211
	Poisson's ratio	0.26
Cement sheath	Elastic modulus (GPa)	9
	Poisson's ratio	0.25

A total of 3 types of research schemes were set for this numerical simulation: ① Spiral perforation scheme: hole density of 16 holes/m, phase angles of 0°, 60°, 90°, 120°; ② Fixed-plane perforation scheme: hole density of 16 holes/m, phase angles of 0°, 45°; ③ Plane perforation scheme: hole density of 16 holes/m, phase angles of 0°, 30°, 60°, 90°. Taking initiation pressure, fracture width and casing Mises stress as the core evaluation indicators, the fracturing effect and casing safety of different perforation technologies and parameters were systematically analyzed.

3. Study on the Influence Laws of Different Perforation Process Parameters

3.1 Influence Laws of Spiral Perforation Parameters

The included angle between two adjacent perforations is the perforation phase angle. Fig.2 is a schematic diagram of the spiral perforation phase angle setting in the numerical simulation calculation process. In this section, under the conditions of aperture of 10 mm and hole density of 16 holes/m, different perforation phase angles (0°, 60°, 90°, 120°) were set, and a rock initiation model for volume

ISSN: 2414-1895 DOI: 10.6919/ICJE.202603_12(3).0046

fracturing after perforation by an 89-type spiral perforator with eight clusters of perforation sections was established to analyze the fracture pressure and study the fracture morphology near the wellbore.

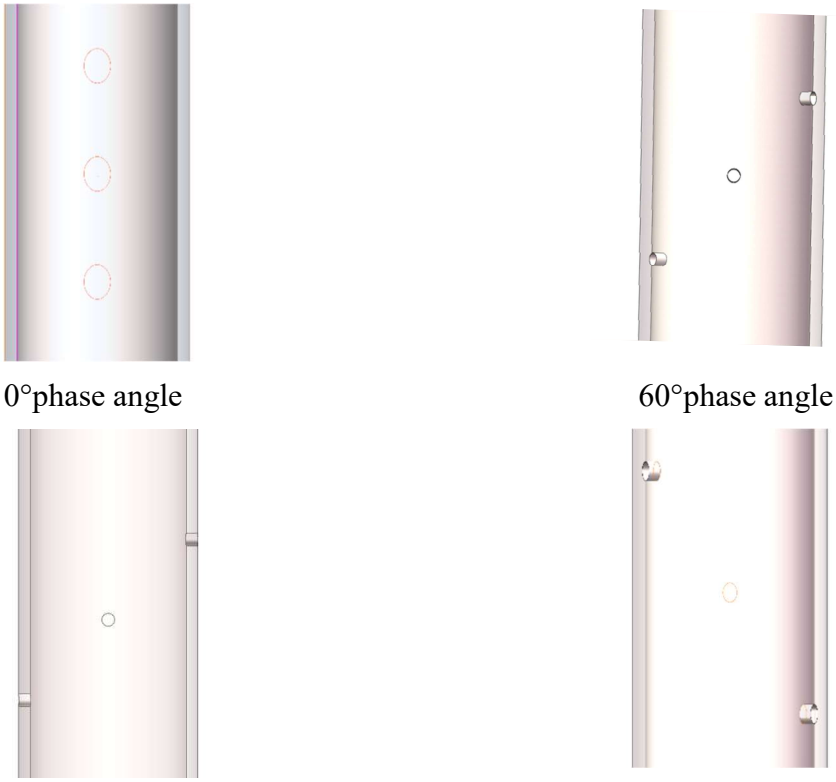

0°phase angle 60°phase angle

90°phase angle 120°phase angle

Fig. 2 Perforation layout of spiral perforation

For the spiral perforation technology, the influence laws of different phase angles on fracture initiation and propagation and casing damage were studied. The numerical simulation results show that the fractures all extend along the direction of the maximum horizontal in-situ stress, and form rectangular fractures finally after the tip initiation, as shown in Fig.3.

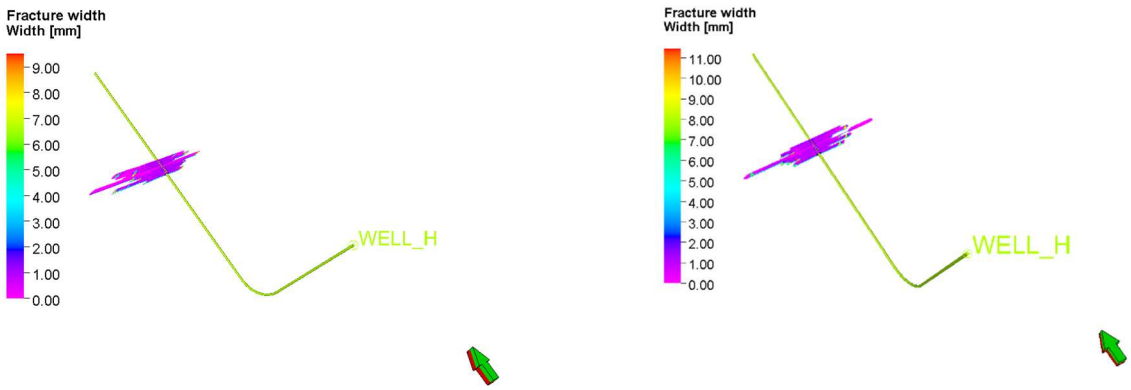

0°phase angle 60°phase angle

ISSN: 2414-1895 DOI: 10.6919/ICJE.202603_12(3).0046

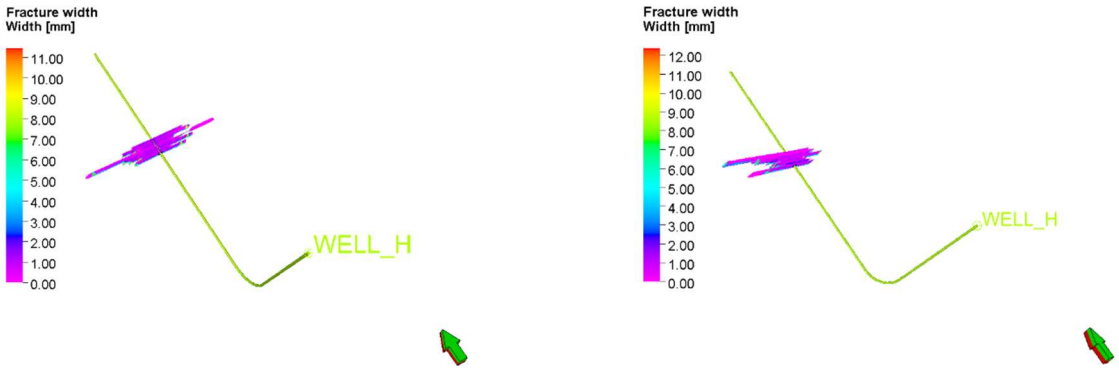

90°phase angle 120°phase angle

Fig. 3 Fracture propagation view of spiral perforation in xoz plane

Fig. 4 shows the curves of initiation pressure with time under four different perforation phase angles respectively. From the calculation results, the fracture pressure has a non-linear relationship with the phase angle, and the change of initiation pressure is not a monotonic function but a multivariate function similar to a U-shape. With the increase of perforation phase angle, the initiation pressure first decreases and then increases, then decreases and finally increases. At 0° phase angle, the initiation pressure is the maximum (86.7 MPa); at 60° phase angle, the initiation pressure is the minimum (70.9 MPa), which is 18.2% lower than that at 0°.

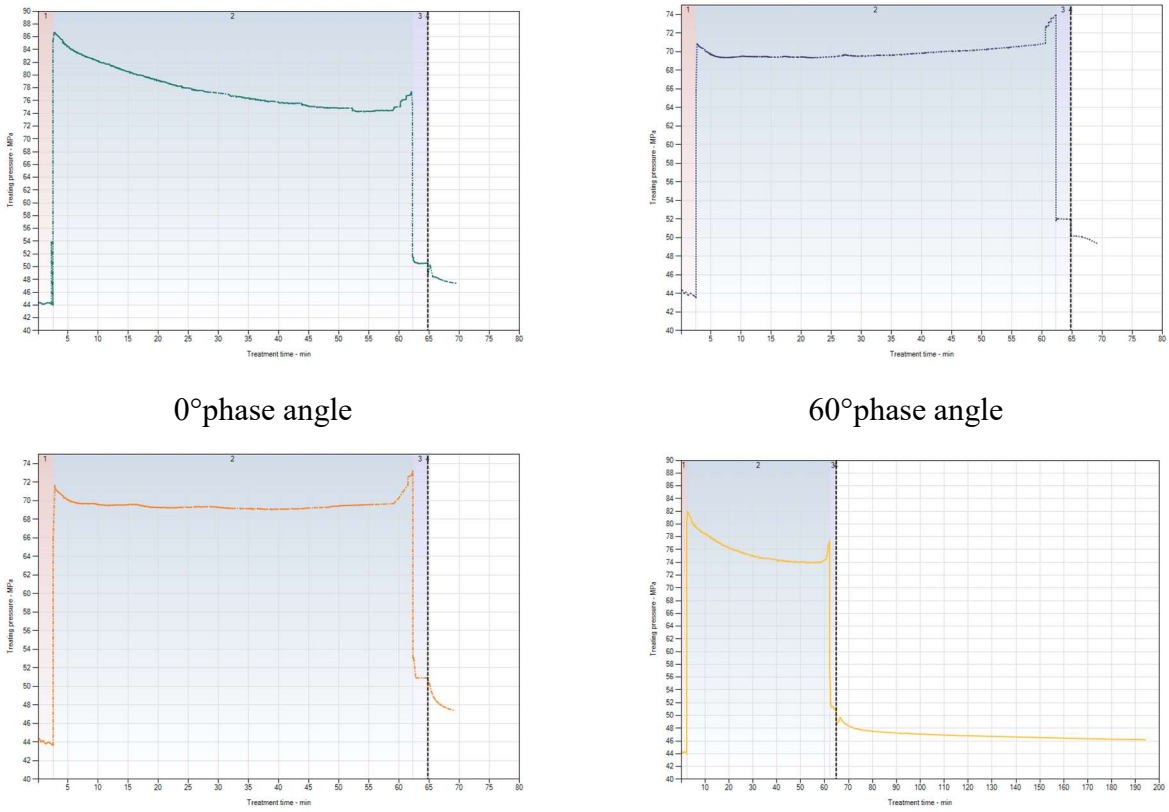

0°phase angle 60°phase angle

90°phase angle 120°phase angle

Fig. 4 Variation curves of initiation pressure under different phase angles

ISSN: 2414-1895 DOI: 10.6919/ICJE.202603_12(3).0046

Under the conditions of casing hole density of 16 holes/m and aperture of 10 mm, a uniformly distributed load increasing gradually was applied to the inner wall surface, and the equivalent stress distribution on the casing surface during the process is shown in Fig.5. It can be seen from the figure that the casing Mises stress is the maximum (726 MPa) at 0° phase angle, close to the yield limit of the casing. Since all holes are arranged along the same spiral line with a small hole spacing, it may lead to a high stress concentration area along the spiral line direction, and the holes are on the same plane, so one side of the casing may bear greater stress, thus increasing the risk of damage; the casing Mises stress is the minimum (600 MPa) at 60° phase angle, which is 17.36% lower than that at 0° phase angle. The holes are distributed in a circle every 60°, with a relatively uniform spiral interval, which can disperse the stress concentration and reduce the local high stress area. At the same time, the spiral arrangement can promote the multi-directional fracture propagation. In the spiral perforation technology, the 60° phase angle significantly reduces the risk of casing damage by optimizing the stress distribution, and forms a complex fracture network with double main fractures intertwined spirally to improve the volume of fracturing reconstruction, which can further ensure the wellbore integrity.

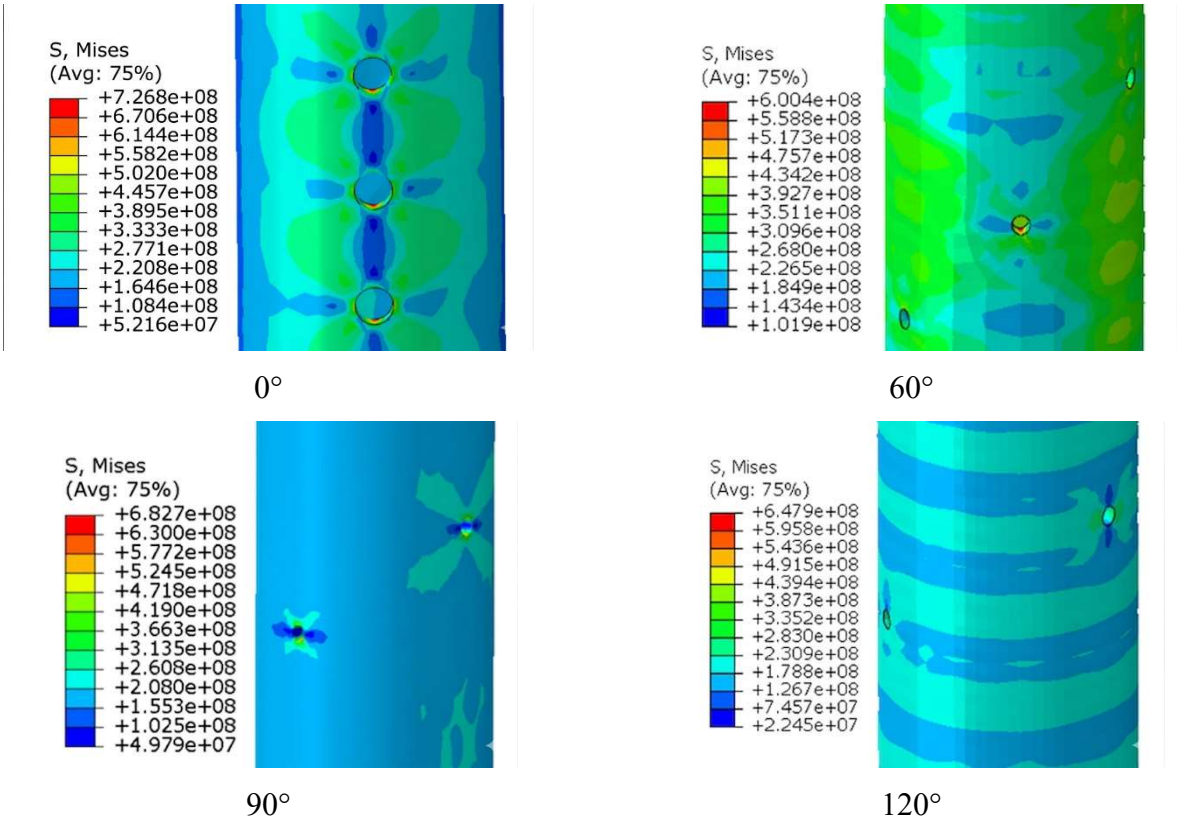

Fig. 5 Casing stress under different perforation phase angles

As shown in Fig.6, with the increase of perforation phase angle, the initiation pressure first decreases and then increases, the fracture width first increases and then decreases, and the Mises stress first decreases and then increases. At 60° phase angle, the initiation pressure is the minimum (70.9 MPa), the fracture width is the maximum (4.88 mm), and the casing Mises stress is the minimum (600 MPa). Therefore, the optimal phase angle of spiral perforation is 60°.

ISSN: 2414-1895 DOI: 10.6919/ICJE.202603_12(3).0046

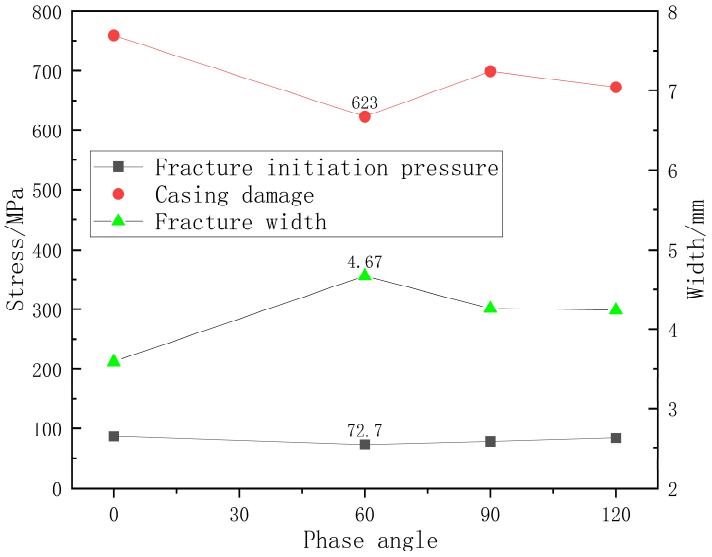

Fig. 6 Variation curves of initiation pressure, fracture width and Mises stress of spiral perforation under different phase angles

3.2 Influence Laws of Fixed-plane Perforation Parameters

Study on the influence laws of fixed-plane perforation technology on formation volume fracturing: Using hydraulic fracturing software and boundary element method, a finite element model of rock initiation for volume fracturing after perforation by an 89-type fixed-plane perforator (aperture of 10 mm, hole density of 16 holes/m, phase angles of 0°, 45°) was established, as shown in Fig.7, with a total of 8 clusters of perforation sections set, to analyze the influence degree and laws of perforation phase angle, hole density and aperture on rock initiation pressure and casing damage. According to the established finite element analysis results, the fracture propagation morphology and laws of rock after perforation by the 89-type fixed-plane perforator with different perforation phase angles, hole densities and apertures were analyzed through the post-processing program.

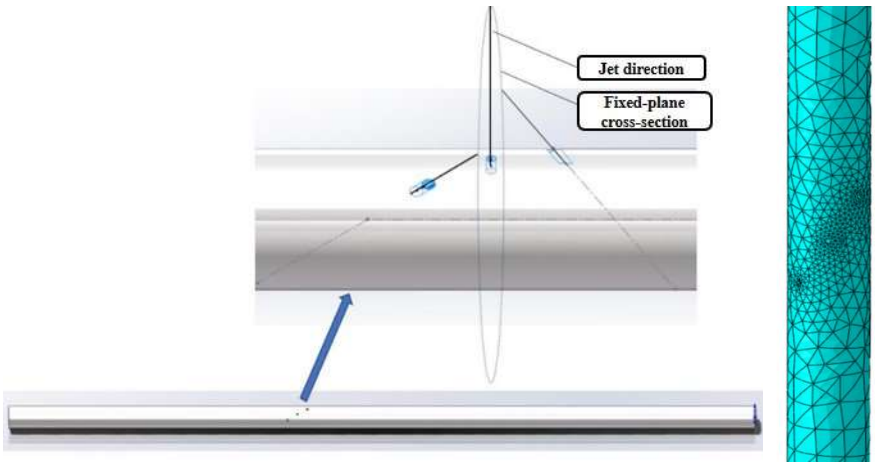

Fig. 7 3D fixed-plane perforation model and mesh

Fig.8 shows the fracture propagation view of fixed-plane perforation in the xoz plane. It can be seen that the length and width of fractures generated by each cluster of perforation sections are irregularly distributed, among which the third cluster of perforation sections has the longest fracture length and the fourth cluster has the shortest.

ISSN: 2414-1895 DOI: 10.6919/ICJE.202603_12(3).0046

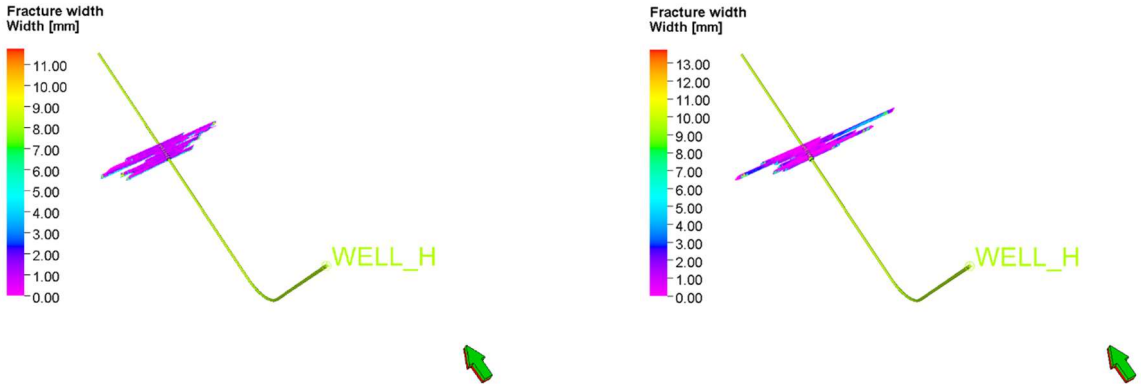

0° 45°

Fig. 8 Fracture propagation view of fixed-plane perforation in xoz plane

Fig. 9 shows the curves of initiation pressure with time. With the increase of fracturing time, the pumping pressure increases, and the pumping pressure increases rapidly at 2.5 s. The tensile stress on the wall surface of the perforation hole exceeds the tensile strength of the rock, at which time the initiation occurs on the wall surface of the perforation hole with an initiation pressure of 67.5 MPa. The initiation pressure drops rapidly and stabilizes at 62.5 s, and the hydraulic fracturing is completed.

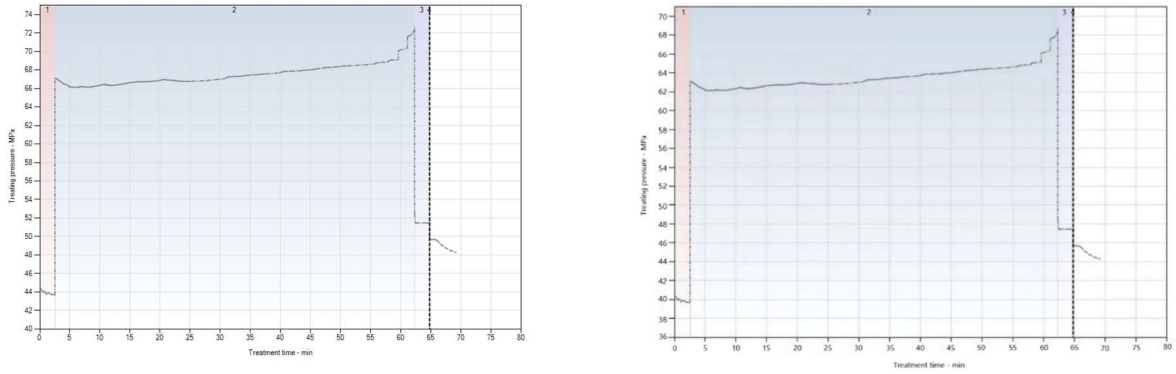

0° 45°

Fig. 9 Variation curves of initiation pressure of fixed-plane perforation under different phase angles

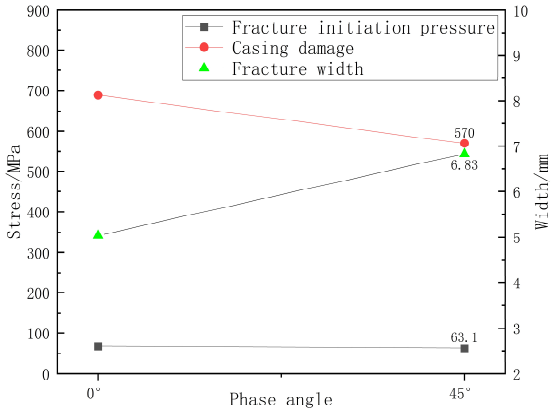

Fig. 10 Variation curves of initiation pressure, fracture width and Mises stress of fixed-plane perforation under different phase angles

ISSN: 2414-1895 DOI: 10.6919/ICJE.202603_12(3).0046

As shown in Fig.10, the initiation pressure at 0° phase angle and 16 holes/m is 67.5 MPa, the maximum fracture width is 5.04 mm, and the maximum Mises stress is 689 MPa; at 45° phase angle and 12 holes/m, the initiation pressure is 63.1 MPa, the maximum fracture width is 6.83 mm, and the maximum casing Mises stress is 570 MPa. Compared with 0° phase angle, 45° phase angle has lower initiation pressure, larger fracture width, better fracturing effect and significant stress dispersion effect.

3.3 Influence Laws of Plane Perforation Parameters

The 3D formation finite element model established is the same as that in Fig.1. Fig.11 is a schematic diagram of the plane perforation phase angle setting in the numerical simulation calculation process. In this chapter, under the condition of aperture of 10 mm and hole density of 16 holes/m, different perforation phase angles (0°, 30°, 60°, 90°) were set to analyze the initiation pressure and study the fracture morphology near the wellbore.

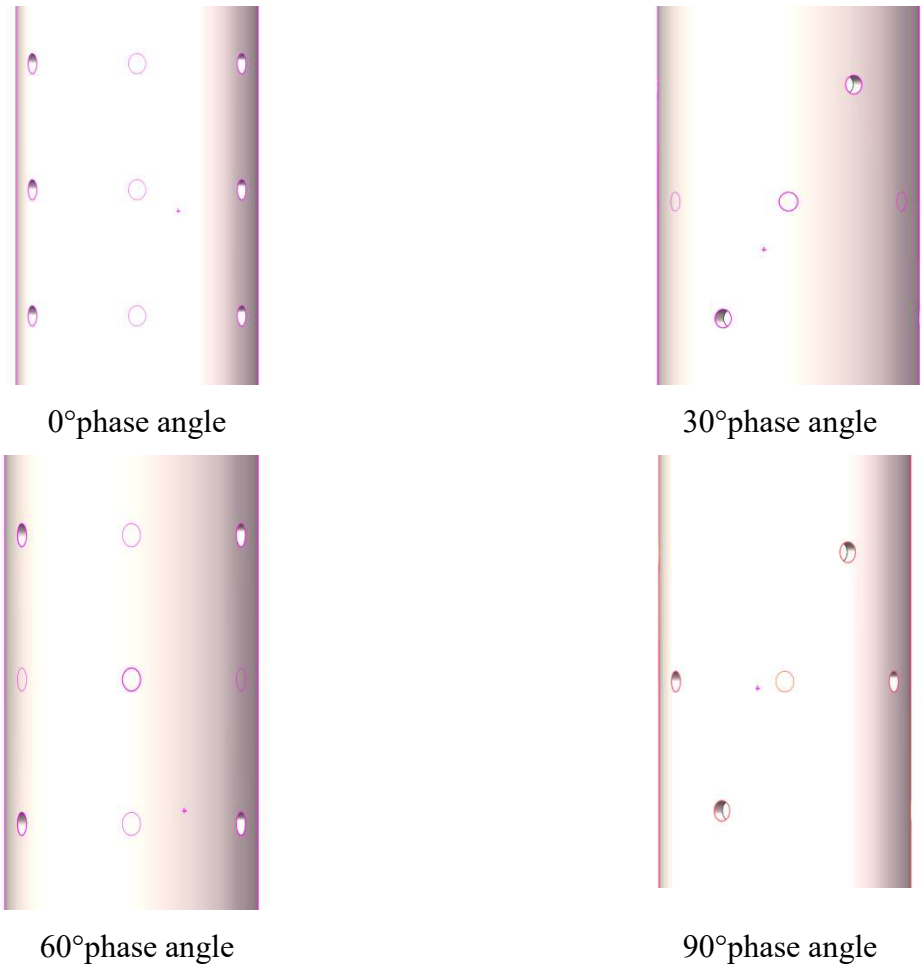

Fig. 11 Perforation layout of plane perforation

Fig.12 shows the fracture propagation views of plane perforation in the xoz plane under four different perforation phase angles respectively. A comprehensive comparison shows that these different fracture propagation morphologies indicate the complexity of fracture propagation near the wellbore. At 30° phase angle, the fracture development is relatively complete due to the low stress concentration near the perforation, and the fracture pressure is relatively low; at 90° phase angle, some perforations only initiate in a small range near the perforation and fail to form an effective diversion channel, so the fracture pressure is relatively high.

ISSN: 2414-1895 DOI: 10.6919/ICJE.202603_12(3).0046

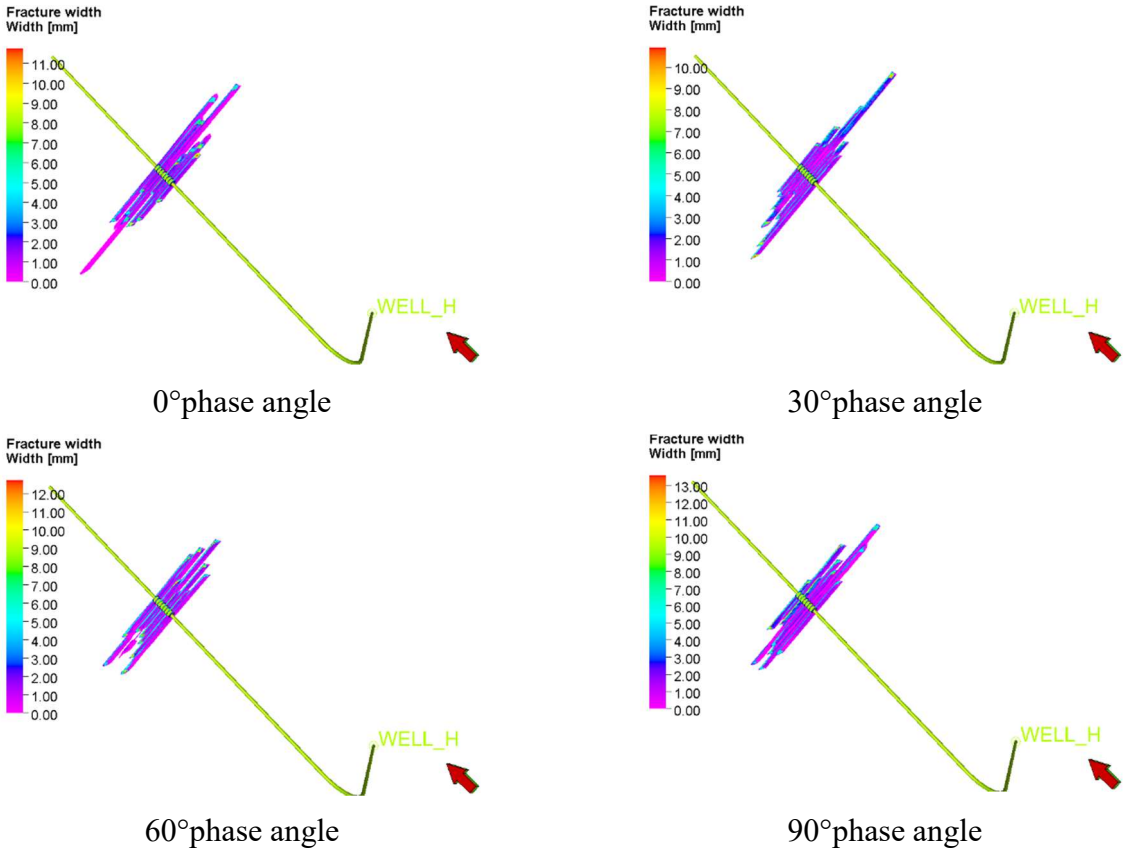

Fig. 12 Fracture propagation view of plane perforation in xoz plane

Fig.13 shows the curves of initiation pressure with time under four different perforation phase angles respectively. With the increase of fracturing time, the pumping pressure increases, and the initiation occurs on the wall surface of the perforation hole at 2.5 s, the initiation pressure increases rapidly, and the initiation pressure drops rapidly and stabilizes at 62.5 s. A comprehensive comparative analysis of Fig.13 shows that with the increase of perforation phase angle, the initiation pressure first decreases and then increases. At 90° phase angle, the initiation pressure is the maximum (81.6 MPa); at 30° phase angle, the initiation pressure is the minimum (61.2 MPa).

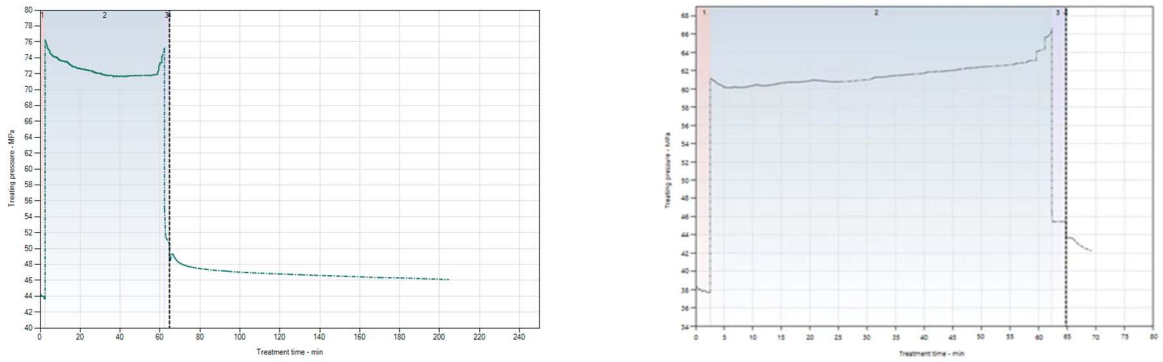

ISSN: 2414-1895 DOI: 10.6919/ICJE.202603_12(3).0046

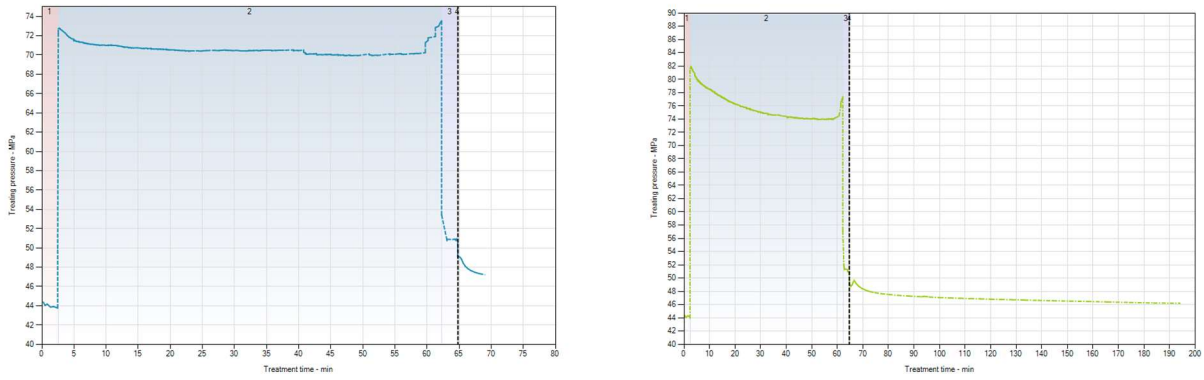

60°phase angle 90°phase angle

Fig.13 Variation curves of initiation pressure of plane perforation under different phase angles

Under the conditions of casing hole density of 16 holes/m, aperture of 10 mm and different perforation phase angles, fixed constraints were applied to the two end faces of the casing, and a uniformly distributed load increasing gradually was applied to the inner wall surface. The equivalent stress distribution on the casing surface during the process is shown in Fig.14. It can be seen from the figure that the casing Mises stress is the maximum (574 MPa) at 0° phase angle, and the minimum (475 MPa) at 90° phase angle, which is 17.2% lower than that at 0°.

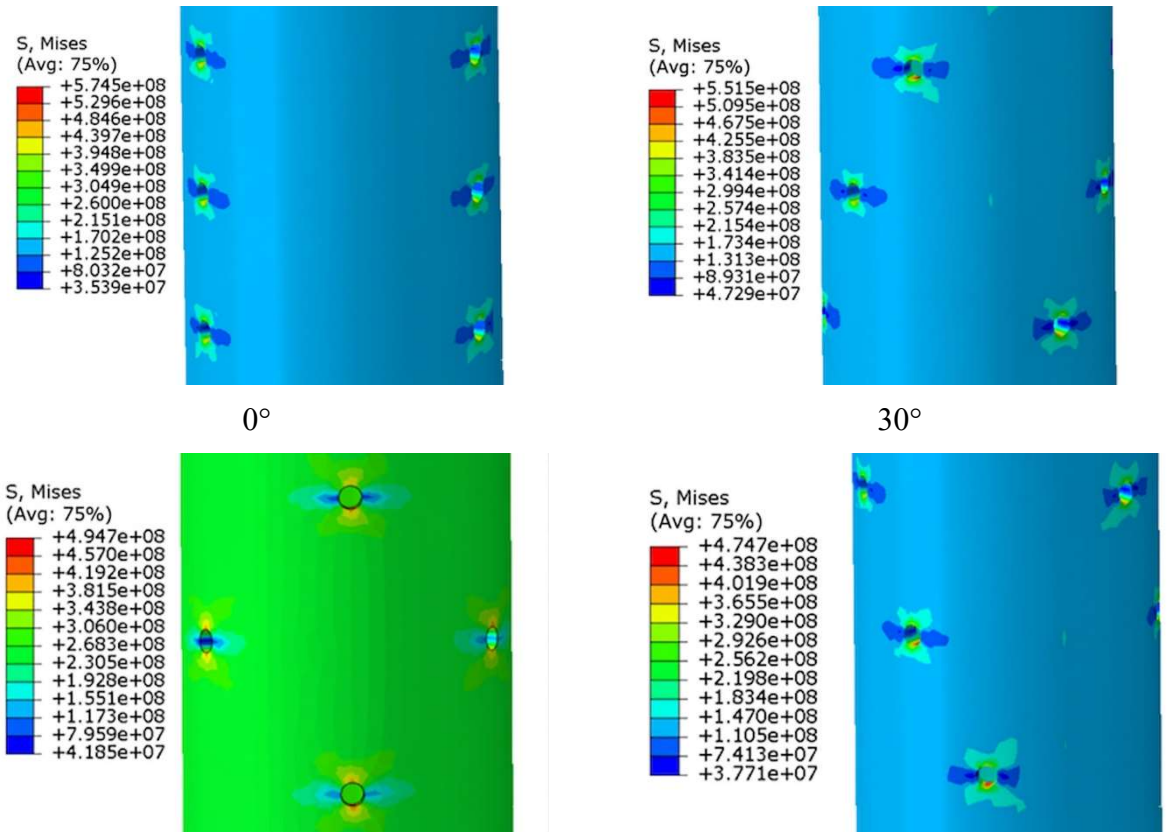

0° 30°

60° 90°

Fig. 14 Casing stress of plane perforation under different perforation phase angles

ISSN: 2414-1895 DOI: 10.6919/ICJE.202603_12(3).0046

As shown in Fig.15, with the increase of perforation phase angle, the initiation pressure first decreases and then increases, the fracture width first increases and then decreases, and the Mises stress decreases gradually. At 30° phase angle, the initiation pressure is the minimum (61.2 MPa), the fracture width is the maximum (5.27 mm), and the casing Mises stress is 551 MPa. Therefore, the optimal phase angle of plane perforation is 30°.

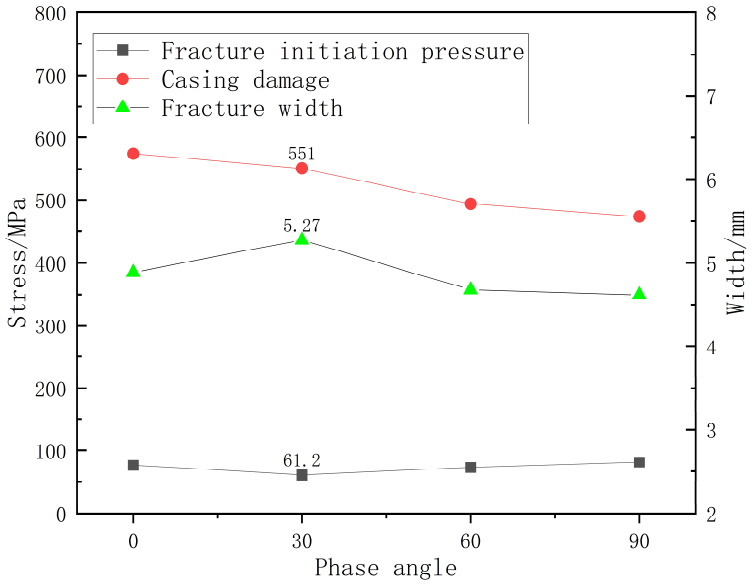

Fig. 15 Variation curves of initiation pressure, fracture width and Mises stress of plane perforation under different phase angles

4. Verification of Physical Model Experiments

4.1 Scheme of True Triaxial Physical Model Experiment

To verify the reliability of the numerical simulation results, a true triaxial hydraulic fracturing simulation system was used to carry out physical model experiments. The system has a maximum confining pressure loading capacity of 50 MPa and a maximum pumping pressure of 70 MPa, which can simulate the whole process of hydraulic fracturing of standard rock samples with the size of 30 cm×30 cm×30 cm. Homogeneous cement samples were used in the experiment to simulate reservoir rocks, as shown in Fig.16. The wellbore and perforation holes were prefabricated by wire cutting technology, and the well wall and the simulated wellbore were bonded with high-strength epoxy resin to ensure the experimental tightness.

Fig. 16 Diagram of cement samples for experiment

ISSN: 2414-1895 DOI: 10.6919/ICJE.202603_12(3).0046

Table 2. Parameter table of physical model experiment scheme

Serial number	Displacement (ml/min)	Aperture (mm)	Hole depth (mm)
1	30	10	6
2	60	10	6
3	90	10	6
4	60	8	6
5	60	12	6
6	60	10	10
7	60	10	14

Seven groups of schemes were set in the experiment, focusing on analyzing the influence of pumping displacement, perforation aperture and perforation hole depth on fracture initiation pressure and propagation morphology, and the experimental parameters are shown in Table 2. The experimental steps are as follows: ① Put the rock sample into the true triaxial cavity and apply three-dimensional confining pressure to the design value; ② Inject fracturing fluid through the ISCO constant flow pump and record the change of pumping pressure with time; ③ Take out the rock sample after the injection and observe and record the fracture morphology and development characteristics. (1) When the perforation azimuth angle θ increases from 0° to 45°, the fracture will deflect while extending; when θ increases from 45° to 90°, the deflection angle of the fracture decreases while extending. The fracture will extend along the perforation direction until the force generated by the pumping pressure cannot fracture the rock formation and the initiation stops.

It can be seen from Fig.17(a) to Fig.17(c) that by increasing the pumping displacement (i.e., increasing the liquid inlet rate and reducing the perforation density), the fracture morphology changes from single-wing fracture initiation to double-wing and multi-fracture initiation, but the larger the displacement, the higher the fracture initiation pressure. It can be seen from Fig.17(b), Fig.17(d) to Fig.17(e) that by increasing the perforation aperture, the fracture morphology is dominated by double-wing fractures and supplemented by branch fracture initiation, and the larger the aperture, the greater the degree of branch fracture generation. The fracture initiation pressure decreases with the increase of aperture, but the degree of decrease is not obvious. It can be seen from Fig.17(b), Fig.17(f) to Fig.17(g) that by increasing the perforation depth, the fracture transitions from vertical fracture to angled and horizontal fracture morphology, and the larger the hole depth, the higher the horizontal degree. The fracture initiation pressure decreases with the increase of hole depth, but the degree of decrease is not obvious.

ISSN: 2414-1895 DOI: 10.6919/ICJE.202603_12(3).0046

(a) Experiment 1

(b) Experiment 2

(c) Experiment 3

(d) Experiment 4

(e) Experiment 5

(f) Experiment 6

(g) Experiment 7

Fig. 17 Diagram of fractured samples in the experiment

ISSN: 2414-1895 DOI: 10.6919/ICJE.202603_12(3).0046

The experimental results of the influence of perforation parameters (displacement, aperture, hole depth) on fracture initiation pressure and fracture morphology are summarized as follows:

Table 3. Experimental results of hydraulic fracturing under different perforation parameters

Serial number	Displacement (ml/min)	Aperture (mm)	Hole depth (mm)	Fracture pressure (MPa)	Number of fractures	Fracture morphology	Fracture strike
1	30	10	6	15.13	1	Single-wing	Vertical
2	60	10	6	16.62	3	Double-wing + branch	Vertical
3	90	10	6	16.67	4	Double-wing + branch	Vertical
4	60	8	6	16.38	3	Double-wing + branch	Vertical
5	60	12	6	16.30	4	Double-wing + branch	Vertical
6	60	10	10	16.85	3	Double-wing + branch	Vertical + horizontal
7	60	10	14	16.79	3	Double-wing + branch	Vertical + horizontal

4.2 Comparison of Physical Model Experiment and Numerical Simulation Results

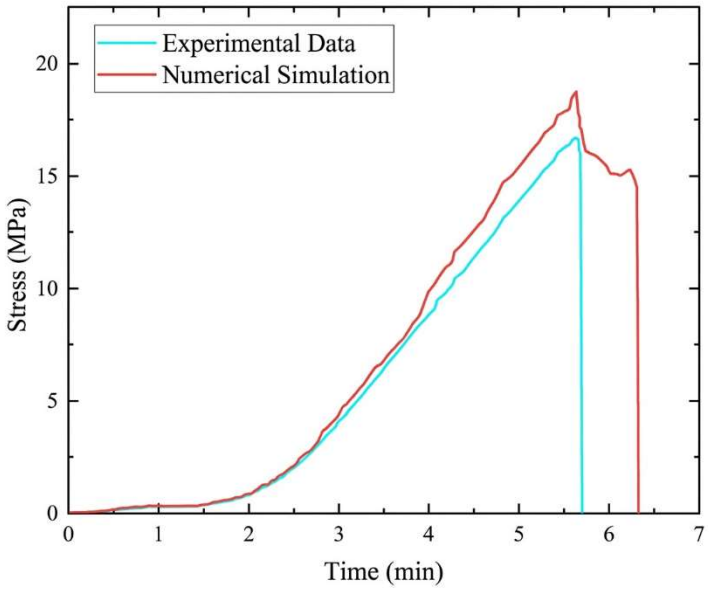

Fig. 18 Comparison of numerical simulation and physical model experiment results

Benchmarking the 3rd group of the physical model experiment, a rock sample model with the size of 30 cm×30 cm×30 cm was established, the maximum three-dimensional stress can be loaded to 50 MPa, and the maximum pumping pressure can reach 70 MPa. Fracturing fluid was injected at a pumping speed of 90 ml/min until the sample fractured, with an aperture of 10 mm and a hole depth

ISSN: 2414-1895 DOI: 10.6919/ICJE.202603_12(3).0046

of 6 mm. The change relationship of initiation pressure with time was obtained and compared with the physical model experiment results, as shown in Fig.18. Compared with the physical model experiment, the two have a good consistency in the overall trend of stress evolution with time: the stress increases gradually with the loading time, and the two curves basically coincide, indicating that the numerical model can reflect the stress accumulation law during fracture propagation more accurately; the fracture starts to initiate at 5.6 s with an initiation pressure of 16.67 MPa, while the numerical simulation result is slightly higher (18.69 MPa) with an error of 12.12%; in the failure stage, the experimental results show a sudden drop of stress to zero rapidly, revealing the characteristics of sudden instability failure, while the numerical simulation shows a relatively slow decline with some residual stress remaining.

5. Conclusion

Through the comprehensive study on the influencing factors and laws of rock initiation pressure and fracture propagation under different perforation technologies such as spiral perforation, fixed-plane perforation and plane perforation, the following conclusions are drawn:

(1) Under the condition of spiral perforation technology, with the increase of perforation phase angle (0°~120°), the initiation pressure first decreases and then increases, the fracture width first increases and then decreases, and the Mises stress first decreases and then increases. When the hole density is 16 holes/m and the phase angle is 60°, the initiation pressure is the minimum (70.9 MPa), the fracture width is the maximum (4.88 mm), and the casing Mises stress is the minimum (600 MPa). Therefore, the optimal phase angle of spiral perforation is 60°.

(2) The optimal fracturing perforation parameters of fixed-plane perforation technology are 45° phase angle and 16 holes/m, at which the initiation pressure is 63.1 MPa, the maximum fracture width is 6.83 mm, and the maximum casing Mises stress is 570 MPa.

(3) Under the condition of plane perforation technology, with the increase of phase angle (0°~90°), the rock initiation pressure first decreases and then increases, the fracture width first increases and then decreases, and the maximum casing Mises stress decreases gradually. Comprehensively, when the phase angle is 30°, the initiation pressure is the minimum (61.2 MPa), the fracture width is the maximum (5.27 mm), and the Mises stress is 551 MPa.

(4) The change relationship of initiation pressure with time was obtained by simulating the pumping speed of 90 ml/min, aperture of 10 mm and hole depth of 6 mm in the physical model experiment. It can be seen that the two have a good consistency in the overall trend of stress evolution with time. The fracture starts to initiate at 5.6 s with an initiation pressure of 16.67 MPa, while the numerical simulation result is slightly higher (18.69 MPa) with an error of 12.12%.

References

[1] Yu Q G. Study on Fracture Propagation Law of Spiral Perforation and Fracturing Optimization in Different Reservoirs[D]. Daqing: Northeast Petroleum University, 2023.

[2] Wang X H, Luo H R, Zhang F S. Parameter optimization for controlling near-wellbore fracture complexity under perforation fracturing completion of horizontal wells[J]. Chinese Journal of Rock Mechanics and Engineering, 2022, 41(06):1223-1234.

[3] Zhao Z F, Tang M R, Pang M Y, et al. Study on the influence of fixed-plane perforation on the initial fracture morphology of fracturing[J]. Science Technology and Engineering, 2016, 16(22):60-63.

[4] Wang S L, Su Y B, Sun Y A, et al. Study on the influence of new fixed-plane perforation technology on casing strength[J]. Mechanics in Engineering, 2018, 40(04):402-408.

[5] Weng D W, Fu H F, Bao L Q, et al. Experimental study on plane perforation of horizontal wells[J]. Natural Gas Geoscience, 2018, 29(04):572-578.

[6] Jiang S, Li Y P, Du F S, et al. Technical progress in improving the gas production rate of perforation clusters in fractured wells of shale gas reservoirs[J]. Reservoir Evaluation and Development, 2023, 13(01):9-22.